Title: mTORC1 controls cytoplasmic crowding by regulating ribosome concentration

Authors: M. Delarue[1†], G. Brittingham[1†], I.V. Surovtsev[2], K.J. Kennedy[3], J.I. Guttierrez[3], J.K. Chung[4], J.T. Groves[4,5], C. Jacobs-Wagner[2,5] and L.J. Holt[1*]

* Correspondence: liam.holt@nyumc.org

† These authors contributed equally

Affiliations:

[1] Institute for Systems Genetics, New York University Langone Medical Center

[2] Department of Molecular, Cellular, and Developmental Biology, Yale University

[3] Department of Molecular and Cell Biology, University of California, Berkeley

[4] Department of Chemistry, University of California, Berkeley

[5] Howard Hughes Medical Institute

* Correspondence to: liam.holt@nyumc.org

[†] These authors contributed equally

Abstract:

Crowding within the cell is optimized to accelerate reactions, but not excessively impede diffusion. However, the mechanisms that regulate crowding are unknown. We developed genetically encoded multimeric (GEM) nanoparticles to study the physical properties of the cytoplasm. GEMs self-assemble into bright, stable fluorescent particles of defined size and shape. We used this system to discover signaling pathways that modulate crowding in yeast and mammalian cells. We found that the mTORC1 pathway tunes macromolecular crowding through regulation of ribosome concentration and thereby regulates the effective diffusion of macromolecules larger than 16 nm in diameter but has no effect on the diffusion of molecules at the 5 nm length-scale, thus providing a mechanism to differentially tune reactions in the cell based on particle size. This tuning of rheology makes induction of a stress response gene more robust to osmotic pressure. Our results connect a central regulator of growth and metabolism to the biophysical properties of the cell.

One Sentence Summary: *(less than 150 characters)*

Using genetically encoded nanoparticles, we find that mTORC1 controls molecular crowding in the cytosol by regulating ribosome concentration.

Main Text:

It is estimated that around 40% of the cytoplasmic volume is taken up by macromolecules (*1*). This molecular crowding is crucial for the efficient function of biological systems: If *Xenopus* extracts are diluted by more than a few percent, fundamental biological processes such as mitosis and DNA replication fail. A high concentration of crowding agents can entropically favor molecular association events, thereby accelerating molecular reactions (*1*, *2*). However, excessive crowding can also dramatically decrease molecular motion, just as the loss of a lane on a freeway can transform smooth traffic flow to instant gridlock (*3*, *4*). This kind of jamming depends strongly on particle size: molecules of equivalent or larger size to the main crowding agent are affected more strongly than small particles that move through the gaps. Thus, changes in molecular crowding can have profound effects on cell physiology and may affect some processes disproportionately while allowing others to proceed, depending on the typical size of molecules in each molecular pathway. However, the mechanisms that control crowding are unknown.

One method to probe the physical properties of the cytoplasm is passive microrheology, in which the viscous and elastic properties, structure, and dynamics of materials are inferred from the motion of tracer particles (*5*, *6*). Various groups have studied the motion of non-biological nanoparticles in cells (*7*, *8*), but these techniques are labor intensive and can perturb the cell. For example, microinjection necessarily disrupts the cell structure and is impossible in organisms like budding yeast. An alternative approach is to trace the motion of endogenous particles such as mRNA (*9*). However, when the motion an endogenous molecule changes, it is difficult to know if this is due to regulation of the properties of the molecule or to changes in the surrounding environment. Orthogonal biological tracers have been used to address this issue, including the μNS particle from avian rheovirus (*10*-*12*). These types of tracer particle are less likely to undergo regulated interactions with the cell, but a major limitation of the μNS system is that it does not have a well-defined shape or size, making precise physical interpretation difficult.

We developed Genetically Encoded Multimeric nanoparticles (GEMs) to address these limitations. GEMs are comprised of a homo-multimerizing scaffold fused to a fluorescent protein. Figure 1A illustrates a GEM built on an encapsulin scaffold from the hyperthermophile *Pyrococcus furiosus* (*13*) fused to green fluorescent protein (GFP). When expressed within cells, 180 copies of this protein self-assemble into bright, stable icosahedral particles that we determined to be 37 nm in diameter by negative stain electron microscopy (figure 1B). Therefore, we term these particles 37nm-GEMs. Multi-subunit assemblies such as the proteasome, ribosomes and chromatin remodeling complexes are of a similar size (figure 1C). These orthogonal, stereotyped nanoparticles facilitate passive microrheology as a method to probe the biophysical properties of the cell at a length-scale that was previously inaccessible.

We expressed 37nm-GEMs in budding yeast and in mammalian cells (figure 1D and 1E, supplemental movies 1 and 2). GEMs are bright enough to allow microrheological analysis by single particle tracking (see Material and Methods). GEMs show similar behavior when expressed in different biological systems - 37nm-GEMs have a median apparent diffusion coefficient of around 0.3 $\mu m^2\ s^{-1}$ in both yeast and mammalian cells, in good agreement with expectations from the literature (*7*) - and

therefore show promise as a microrheological standard (figure 2). From the ensemble-averaged mean-squared displacement (MSD), we saw that GEMs do not adhere to typical Brownian motion (figure S1), but rather show anomalous subdiffusive behavior as indicated by a sublinear mean square displacement (MSD, inset figure 2A-B). Subdiffusive motion can indicate a crowded environment and/or interactions of the tracer particle with the environment (*14*). We can compare thousands of individual traces by fitting the initial 100 ms of each trajectory with a linear function $MSD(\tau) = 4D\tau$ to extract the apparent coefficient of diffusion, D, at short timescales.

We observed very different diffusion coefficients for GEMs depending on cell culture conditions. Indeed, when yeast cultures reached saturation, we found that the effective diffusion rates of GEMs increased (figure S2A). By supplementing and depleting various growth medium components (not shown), we found that this accelerated diffusion occurred in response to amino acid depletion (figure S2B).

The mechanistic target of rapamycin complex (mTORC1) is the major amino acid sensor in eukaryotes (*15*). Therefore, we hypothesized that mTORC1 signaling might be responsible for the observed change in cytoplasmic rheology. mTORC1 can be inhibited by addition of rapamycin, which forms an inhibitory complex with the protein FKBP12 (encoded by *FPR1* in *S. cerevisiae*) (*16*). Consistent with our hypothesis, 37nm-GEMs accelerated upon inhibition of mTORC1 with rapamycin in both *S. cerevisiae* and HEK293 cells (figure 2A-B, supplemental movies 1 and 2). Changes in the distribution of coefficients of diffusion were highly significant according to a Kolmogorov-Smirnov test ($p < 1 \times 10^{-41}$ for yeast and $p < 1 \times 10^{-7}$ for HEK293).

We studied other particles to check the generality and length-scale dependence of the changes in microrheology downstream of mTORC1 signaling. We developed a 16nm-GEM based on a lumazine synthase scaffold from *Aquifex aeolicus* (*17*). The diffusion of these 16nm-GEMs also increased upon mTORC1 inhibition. We also saw an increase in the diffusion coefficients of larger structures, such as the endogenous *GFA1* mRNP tagged with the PP7-GFP system (*11*), and of GFP-μNS particles (figure S3). These particles are approximately 100 nm and 200 nm in diameter respectively. To probe rheology at shorter length-scales, we used fluorescence correlation spectroscopy to calculate the effective diffusion of a double-GFP molecule, which is around 5 nm in diameter. The diffusion of this smaller protein was unaffected by the addition of rapamycin (figure S4). Thus, mTORC1 inhibition increases the diffusion coefficients of particles at or above the typical size of multimeric protein complexes, but particles which are the typical size of monomeric proteins or smaller are unaffected. Together, these results are consistent with the hypothesis that mTORC1 regulates the abundance of a major crowding agent of around 16-37 nm in diameter.

We performed additional rheological analysis to better understand how the cytoplasm changes upon mTORC1 inhibition. We found that the step size distribution for 37nm-GEMs is roughly exponential and the typical step size increases upon rapamycin treatment (figure 2C-D). This exponential distribution can be a signature of a fluctuating heterogeneous environment (*14*). The distribution of angles measured between two consecutive steps shows a propensity to go backwards (figure 2E-F), as expected in a crowded or structured environment (*18*). This angle distribution did not change upon rapamycin treatment. Taken together, these observations suggest that

37nm-GEMs are diffusing in a crowded environment that gets diluted upon mTORC1 inhibition.

mTORC1 inhibition causes cells to increase in volume due to continued growth during cell cycle arrest (*19*). Quantification by image analysis showed that cytoplasmic volume increased as diffusion rates increased (figure 3A). However, when we prevented cell division by inhibition of the *cdc28-as* allele of Cyclin Dependent Kinase 1 with the chemical inhibitor 1-NM-PP1, there was no increase in 37nm-GEM motion even though cytoplasmic volume increased. Thus, volume increase alone is not sufficient for the observed cytoplasmic dilution.

We therefore took a genetic approach to expand our investigation. The rapid diffusion of GEMs means that experiments to probe the rheology of the cytoplasm only take a few seconds (for 37nm-GEMs, we imaged at more than 100 Hz to acquire 400 frames in 4 seconds). Thus, we were able to rapidly screen candidate genes to determine the mTORC1-dependent processes that control cellular microrheology (Table S4). As a control, an *fpr1*Δ mutant shows complete epistasis and prevents the effect of rapamycin, indicating a canonical mechanism of action for rapamycin (figure 3B).

Deletion of the gene encoding a major transcription factor for ribosomal RNA biogenesis, *SFP1* (*20*), increased basal diffusion of 37nm-GEMs (figure 3B, right). Disruption of genes encoding the PP2A phosphatase subunit, *SIT4*, and the S6-kinase, *SCH9* – components of the signaling cascade that connects mTORC1 to ribosome biogenesis (*21*, *22*) – also increased basal diffusion coefficients (figure 3B, right). Furthermore, the *sit4*Δ and *sfp1*Δ mutants were both highly epistatic with rapamycin treatment (figure 3B, left). Mutants in *ATG13, ATG17, ATG1* and *RIM15* also showed significant epistasis with rapamycin treatment (figure 3B, right). These genes are all involved in autophagy (*23*), the latter, being especially important for ribophagy (*24*). Thus, mutants that either affected the baseline rate of GEM diffusion and/or showed epistasis with rapamycin treatment fell into two general classes: ribosome biogenesis and autophagy. Ribosomes are one of the most abundant macromolecules in the cytoplasm (*25*, *26*) and are roughly 30 nm in diameter (*27*), consistent with the length-scale dependence of the crowding effects that we observe. Together, this analysis suggests that mTORC1 controls macromolecular crowding by tuning ribosome concentration, and possibly the concentration of downstream proteins.

We synthesized these data in a model of cytoplasmic crowding control (see SI for full details) in which the effective viscosity experienced by a tracer particle, and thus its effective diffusion coefficient, depends on the volume fraction of a major crowding agent. Osmotic perturbation experiments were consistent with this idea and suggested that the volume fraction of the major crowder would correspond to about 40% of all macromolecules (figure S5). Our genetic experiments suggested that either ribosomes, downstream proteins or both could be the major crowder that is perturbed upon rapamycin treatment. We therefore used cyclohexamide treatment to assess the effects of decreased translation alone. Addition of cyclohexamide to cultures did not affect 37nm-GEM mobility (figure 3A), indicating that decreased protein production does not explain our results. Therefore, we postulated that ribosomes *per se* are the main crowding agent regulated by mTORC1. We developed a mathematical framework to explicitly assess this hypothesis. Our model states that under homeostatic conditions,

the specific rate of ribosome production must balance the specific rate of cell growth in order for crowding to remain constant. mTORC1 inhibition breaks this homeostasis by decreasing ribosome production and increasing degradation (*28*), while cell volume continues to increase. From the work of Pestov *et al*, (*28*) we calculated the specific rate of ribosome degradation during rapamycin treatment to be -0.083 +/- 0.03 h^{-1}, which roughly corresponds to an 8% decrease in ribosome number during the first hour. From cell volume measurements, we calculated the specific cell growth rate in rapamycin to be 0.13+/-0.05 h^{-1}, thus cell volume increases roughly 13% in the first hour. The combination of these effects leads to a 20% reduction in ribosome concentration in the first hour of rapamycin treatment. Figure 3C (dashed line) shows that the prediction of our model for the change in diffusion coefficients during mTORC1 inhibition is in excellent agreement with our data on the timescale of minutes to hours. This result supports the hypothesis that changes in ribosome concentration are the predominant mechanism by which mTORC1 regulates cellular rheology (figure 3D).

We hypothesized that the reduction in macromolecular crowding upon mTORC1 inhibition might be adaptive in some conditions. mTORC1 activity is reduced in starvation conditions (*29*), therefore we studied the induction of the starvation response gene Alcohol Dehydrogenase (*ADH2*) upon acute carbon starvation in yeast. We either pretreated cells for 2h with rapamycin to inhibit mTORC1 and therefore decrease cytoplasmic crowding, or used vehicle (DMSO) control. We then acutely withdrew glucose from the media and assayed the ability of yeast cells to induce an mCherry reporter from the *ADH2* promoter at the endogenous locus while varying macromolecular crowding in the cell through a range of osmotic challenges. After inhibition of mTORC1, efficient gene induction occurred over a wider range of sorbitol concentrations than in control cells (figure 4). Thus, the decrease in crowding due to mTORC1 inhibition makes the induction of this stress response gene more robust to osmotic perturbation.

Dramatic changes in cytoplasmic rheology have previously been observed in response to changes in cellular energy state and metabolism. Depletion of ATP in *E. coli* leads to a glass-transition that greatly reduces macromolecular mobility (*10*); glucose starvation in yeast leads to a loss of cell volume and a decrease in the effective diffusion of mRNPs and chromosomal loci due to increased molecular crowding (*11*); and decrease in cytoplasmic pH leads to a gel transition in the cytosol of yeast, associated with entry into a dormant state (*12*). All of these responses decrease the fluidity of the cytosol. Our current work using GEM nanoparticles identifies mTORC1 as a regulator of cytoplasmic crowding in both yeast and mammalian cells. In contrast to carbon starvation, ATP depletion, and acidification, inhibition of mTORC1 accelerates the diffusion of macromolecules. mTORC1 tunes the rheological properties of the cytoplasm by changing the concentration of ribosomes, which are one of the most abundant macromolecules in the cell (around 200,000 ribosomes per yeast cell (*25*); 3,000,000 per HeLa cell (*26*)), occupying up to 40% of the cytoplasmic volume. Thus, in addition to their role in translation, we determine that ribosomes regulate the biophysical properties of the cell. The size of ribosomes sets the length-scale dependence of changes in diffusion and provides the potential for specific downstream physiological changes. In principle, any reaction that requires the passive encounter of two or more complexes of >16 nm will be linked to mTORC1 activity, while reactions that involve

smaller particles (of the typical size of monomeric proteins) or use active transport will be unaffected.

References and Notes:

1. H.-X. Zhou, G. Rivas, A. P. Minton, Macromolecular crowding and confinement: biochemical, biophysical, and potential physiological consequences. *Annu Rev Biophys*. **37**, 375–397 (2008).

2. G. Rivas, J. A. Fernández, A. P. Minton, Direct observation of the enhancement of noncooperative protein self-assembly by macromolecular crowding: indefinite linear self-association of bacterial cell division protein FtsZ. *Proc Natl Acad Sci USA*. **98**, 3150–3155 (2001).

3. A. Miermont *et al.*, Severe osmotic compression triggers a slowdown of intracellular signaling, which can be explained by molecular crowding. *Proceedings of the National Academy of Sciences*. **110**, 5725–5730 (2013).

4. V. Trappe, V. Prasad, L. Cipelletti, P. N. Segre, D. A. Weitz, Jamming phase diagram for attractive particles. *Nature*. **411**, 772–775 (2001).

5. M. A. Mourão, J. B. Hakim, S. Schnell, Connecting the dots: the effects of macromolecular crowding on cell physiology. *Biophys J*. **107**, 2761–2766 (2014).

6. D. Wirtz, Particle-tracking microrheology of living cells: principles and applications. *Annu Rev Biophys*. **38**, 301–326 (2009).

7. K. Luby-Phelps, D. L. Taylor, F. Lanni, Probing the structure of cytoplasm. *J Cell Biol*. **102**, 2015–2022 (1986).

8. B. R. Daniels, B. C. Masi, D. Wirtz, Probing single-cell micromechanics in vivo: the microrheology of C. elegans developing embryos. *Biophys J*. **90**, 4712–4719 (2006).

9. Y. Shav-Tal *et al.*, Dynamics of Single mRNPs in Nuclei of Living Cells. *Science*. **304**, 1797–1800 (2004).

10. B. R. Parry *et al.*, The bacterial cytoplasm has glass-like properties and is fluidized by metabolic activity. *Cell*. **156**, 183–194 (2014).

11. R. P. Joyner *et al.*, A glucose-starvation response regulates the diffusion of macromolecules. *elife*. **5**, e09376 (2016).

12. M. C. Munder *et al.*, A pH-driven transition of the cytoplasm from a fluid- to a solid-like state promotes entry into dormancy. *elife*. **5**, e09347 (2016).

13. F. Akita *et al.*, The crystal structure of a virus-like particle from the hyperthermophilic archaeon Pyrococcus furiosus provides insight into the

evolution of viruses. *J Mol Biol*. **368**, 1469–1483 (2007).

14. B. Wang, J. Kuo, S. C. Bae, S. Granick, When Brownian diffusion is not Gaussian. *Nat Mater*. **11**, 481–485 (2012).

15. K. Hara *et al.*, Amino acid sufficiency and mTOR regulate p70 S6 kinase and eIF-4E BP1 through a common effector mechanism. *J Biol Chem*. **273**, 14484–14494 (1998).

16. J. Heitman, N. R. Movva, M. N. Hall, Targets for cell cycle arrest by the immunosuppressant rapamycin in yeast. *Science*. **253**, 905–909 (1991).

17. X. Zhang, W. Meining, M. Fischer, A. Bacher, R. Ladenstein, X-ray structure analysis and crystallographic refinement of lumazine synthase from the hyperthermophile Aquifex aeolicus at 1.6 A resolution: determinants of thermostability revealed from structural comparisons. *J Mol Biol*. **306**, 1099–1114 (2001).

18. S. Burov, J.-H. Jeon, R. Metzler, E. Barkai, Single particle tracking in systems showing anomalous diffusion: the role of weak ergodicity breaking. *Phys Chem Chem Phys*. **13**, 1800–1812 (2011).

19. Y.-H. M. Chan, W. F. Marshall, Organelle size scaling of the budding yeast vacuole is tuned by membrane trafficking rates. *Biophys J*. **106**, 1986–1996 (2014).

20. I. Fingerman, V. Nagaraj, D. Norris, A. K. Vershon, Sfp1 plays a key role in yeast ribosome biogenesis. *Eukaryotic Cell*. **2**, 1061–1068 (2003).

21. C. J. Di Como, K. T. Arndt, Nutrients, via the Tor proteins, stimulate the association of Tap42 with type 2A phosphatases. *Genes Dev*. **10**, 1904–1916 (1996).

22. R. T. Peterson, B. N. Desai, J. S. Hardwick, S. L. Schreiber, Protein phosphatase 2A interacts with the 70-kDa S6 kinase and is activated by inhibition of FKBP12-rapamycinassociated protein. *Proc Natl Acad Sci USA*. **96**, 4438–4442 (1999).

23. M. Tsukada, Y. Ohsumi, Isolation and characterization of autophagy-defective mutants of Saccharomyces cerevisiae. *FEBS Lett*. **333**, 169–174 (1993).

24. T. M. Waliullah *et al.*, Rim15 and Sch9 kinases are involved in induction of autophagic degradation of ribosomes in budding yeast. *Biosci Biotechnol Biochem*. **81**, 307–310 (2017).

25. J. R. Warner, The economics of ribosome biosynthesis in yeast. *Trends Biochem Sci*. **24**, 437–440 (1999).

26. R. Duncan, J. W. Hershey, Identification and quantitation of levels of protein

synthesis initiation factors in crude HeLa cell lysates by two-dimensional polyacrylamide gel electrophoresis. *J Biol Chem*. **258**, 7228–7235 (1983).

27. J. Mahamid *et al.*, Visualizing the molecular sociology at the HeLa cell nuclear periphery. *Science*. **351**, 969–972 (2016).

28. D. G. Pestov, N. Shcherbik, Rapid cytoplasmic turnover of yeast ribosomes in response to rapamycin inhibition of TOR. *Mol Cell Biol*. **32**, 2135–2144 (2012).

29. R. Zoncu, A. Efeyan, D. M. Sabatini, mTOR: from growth signal integration to cancer, diabetes and ageing. *Nat. Rev. Mol. Cell Biol.* **12**, 21–35 (2011).

Acknowledgements:

We thank Christophe Renou, William Ludington, David Truong, Sudarshan Pinglay, David Savage and Jan Skotheim for discussion and help with the manuscript. We thank David Drubin, Karsten Weis, Jeremy Thorner and Douglas Koshland for advice, strains, plasmids and reagents.

Figure 1

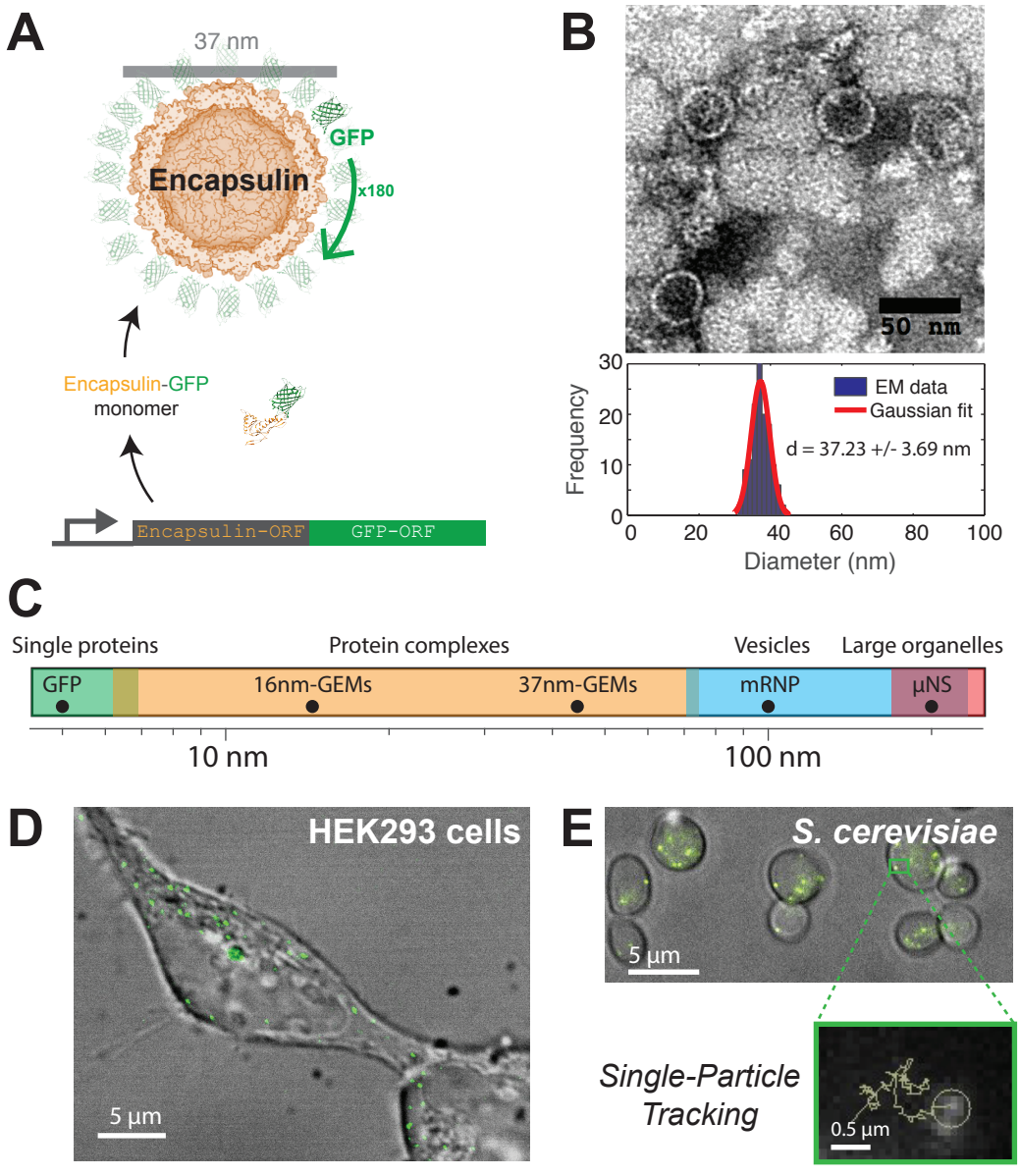

Fig. 1. GEM nanoparticles self assemble to a stereotyped size and can be expressed in budding yeast and mammalian cells. (**A**) Molecular model of genetically encoded multimeric nanoparticles (GEMs) consisting of the *Pyroccocus furiosus* encapsulin protein fused to GFP. (**B**) Negative stain electron microscopy of *Pyroccocus furiosus* encapsulin GEMs purified from yeast cells shown together with quantification showing a median diameter of 37.23 +/- 3.69 nm. (**C**) GEM nanoparticles stably expressed in HEK293 cells. (**D**) GEM nanoparticles expressed in the budding yeast *Saccharomyces cerevisiae* together with single particle tracking at 100 Hz.

Figure 2

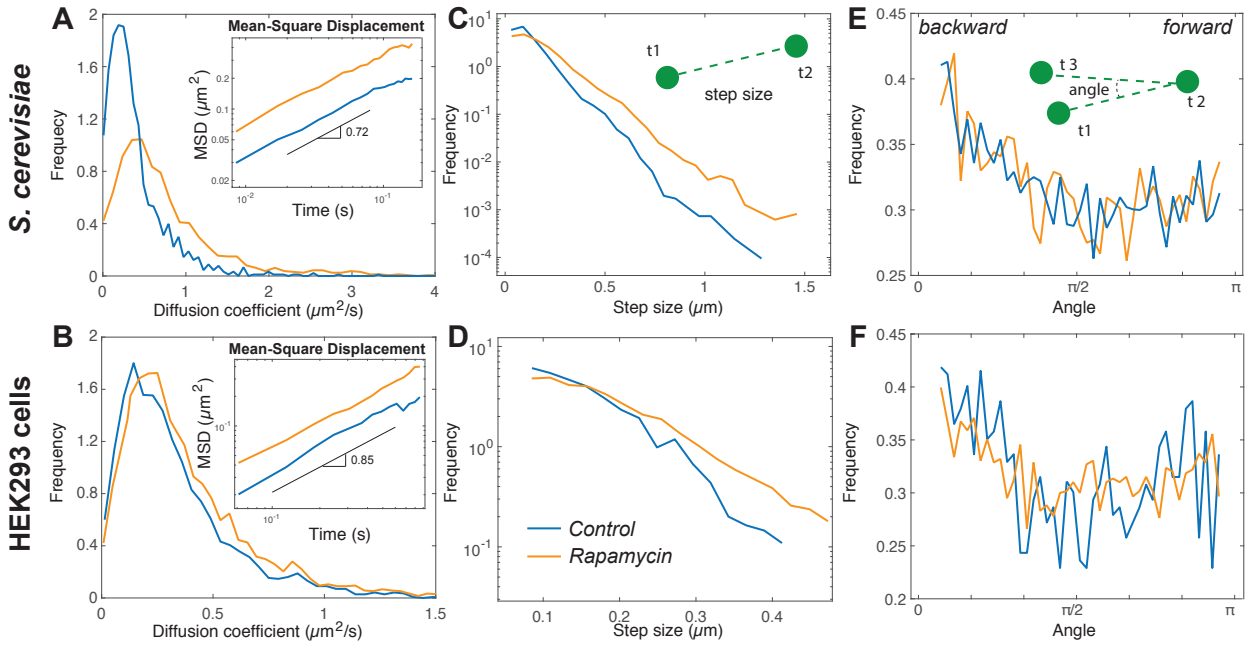

Fig. 2. mTORC1 inhibition increases the rate of GEM diffusion. (**A** and **B)** The distribution of instantaneous diffusion coefficients from the first 100 ms of each trajectory, together with ensemble-averaged mean-square displacements in log-log space (inset) of 37nm-GEMs in control (blue) and rapamycin treatment (orange) conditions for yeast (A) and HEK293 human cells (**B**). Untreated is significantly different from rapamycin according to the 2-sample Kolmogorov-Smirnov test ($p< 1 \times 10^{-41}$ for *S. cerevisiae* and $p < 1 \times 10^{-7}$ for HEK293 cells) (**C** and **D**) Step-size distributions for control (blue) and rapamycin treated yeast (orange) (**C**) and HEK293 cells (**D**). (**E** and **F**) Angle distributions for two sequential steps, for yeast (**E**) and HEK293 cells (**F**).

Figure 3

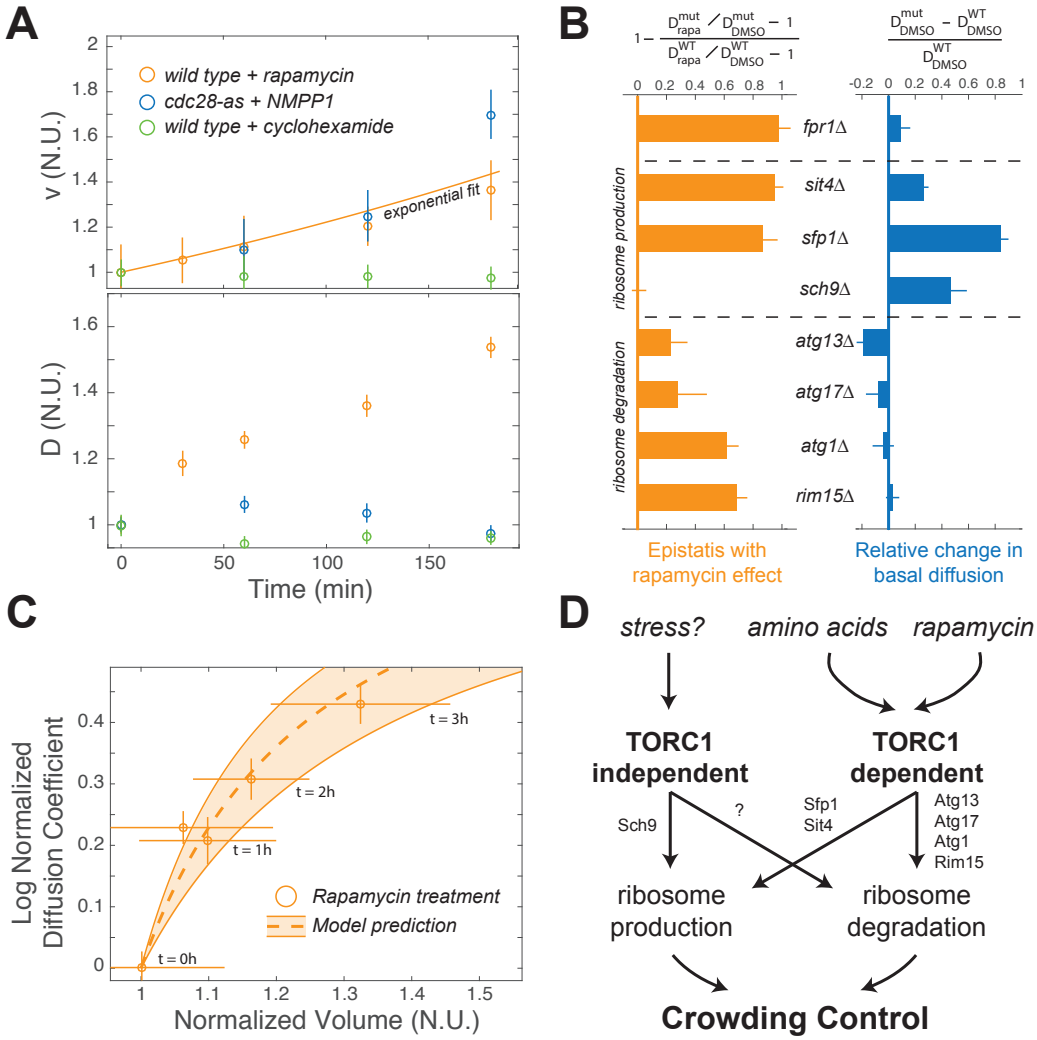

Fig. 3. Genetic analysis suggests that mTORC1 regulates cytoplasmic crowding through regulation of ribosome concentration. (**A**) Change in normalized volume (top) and coefficient of diffusion (bottom) over time for rapamycin treatment (orange) inhibition of cell cycle (blue) and cycloheximide treatment (green). (**B**) Fractional decrease in the effects of rapamycin (epistasis) of various mutants relative to wild type cells (left), and change in the baseline diffusion coefficients of 37nm-GEMs in various genetic backgrounds relative to wild-type cells (right). (**C**) Changes in diffusion as a function of changes in cell volume after mTORC1 inhibition with rapamycin. Data points plus standard error of the mean plotted alongside with model prediction (dashed lines). Shaded area represents the upper and lower limits of the prediction due to uncertainty in the model parameters. (**A bottom**) (**D**) Schematic of pathways that contribute to the regulation of crowding based on genetic evidence presented in B.

Figure 4

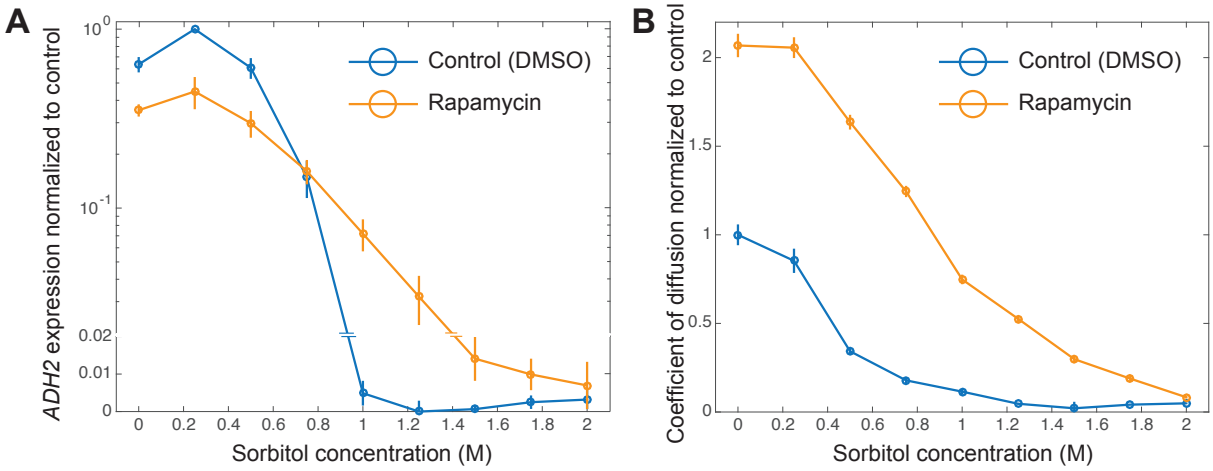

Fig. 4. The induction of the ADH2 gene is more robust to osmotic stress after inhibition of mTORC1. (**A**) ADH2 expression (median induction level of a P_{ADH2}-mCherry reporter) in response to acute carbon starvation at various concentrations of sorbitol (normalized to maximum induction level in vehicle control) (**B**) Median effective diffusion coefficients of 37nm-GEMs (normalized to diffusion coefficients of vehicle control with no sorbitol). DMSO vehicle control is shown in blue and cells pretreated for 2 hours with rapamycin prior to carbon starvation are shown in orange.